Dynamic Manning's roughness coefficients for hydrological modelling in basins

Aizhong Ye, Zheng Zhou, Jinjun You, Feng Ma and Qingyun Duan

ABSTRACT

Manning's roughness coefficient (*n*) has a significant impact on routing in hydrological models. However, computational methods for dynamic roughness coefficients are of little concern in current research. Few studies have produced spatial-temporal distributions of the roughness coefficients in basins. In this study, a formula to calculate the *n* value was established based on a statistical analysis of estimated *n* values by Manning's formula. The routing model of a distributed hydrological model was then improved using the new formula to calculate *n*. The roughness coefficient is not a constant; instead, it changes dynamically with changes in water depth and vegetation in the improved hydrological model. The improved model was applied to the Yellow River basin. The results show that using dynamic *n* can improve the streamflow simulation of hydrological models, especially on slopes. The dynamic spatial-temporal distribution of *n* can now be used in other models.

Key words | dynamic Manning's roughness coefficients, hydrological model, spatial-temporal distribution, Yellow River basin

Aizhong Ye (corresponding author)
Zheng Zhou
Feng Ma
Qingyun Duan
State Key Laboratory of Earth Surface and Ecological Resources, Institute of Land Surface System and Sustainable Development, Faculty of Geographical Science,
Beijing Normal University,
Beijing 100875,
China
E-mail: *azye@bnu.edu.cn*

Jinjun You
State Key Laboratory of Simulation and Regulation of Water Cycle in River Basin,
China Institute of Water Resources and Hydropower Research,
Beijing 100038,
China

INTRODUCTION

Most recently used routing models have been based on the Saint Venant equations or their approximations, such as a kinematic wave, noninertia wave, linear diffusion-wave (Wang *et al.* 2014) and quasi-steady dynamic wave (Reggiani *et al.* 2014). Manning's roughness coefficient, *n*, is one of the most important parameters in hydrological calculations representing the loss of energy in open channels. It is commonly used to calculate discharge and flood water elevations (Coon 1995). Usually, the *n* value is a parameter of the routing module in a hydrological model, Manning's formula is used to calculate discharge and flood levels in equilibrium conditions. The value of *n* has an important effect on the accuracy of the simulated streamflow. However, *n* is difficult to obtain in natural basin (channels and slopes) because it incorporates many factors including vegetation density, riverbed irregularity, surface water width and soil component differences, which contribute to the resistance of flow. The values of Manning's roughness coefficients are different in channel and slopes, the main cause being that the landscape surface in slopes is rougher than channel (Cowan 1956; Azamathulla & Jarrett 2013). Hence, substantial attention has been focused on the roughness coefficient calculations in natural basins.

Generally, estimating the *n* value is subjective. Arcement & Schneider (1989) presented tables of *n* values corresponding to different conditions. A general *n* value of various boundaries is shown at http://www.fhwa.dot.gov/engineering/hydraulics/pubs/2008090/appb.cfm. However, this general *n* value is only an empirical coefficient that does not support quantitative calculation in a hydrological model. To quantitatively present the *n* value, the most widely used formula is Manning's formula if the observed velocity of the flow, hydraulic radius and friction slope can be obtained, as follows:

$$n = R^{2/3} S_f^{1/2} / v \tag{1}$$

doi: 10.2166/nh.2018.175

where v is the velocity of the flow (m/s), n is the Manning's roughness coefficient, R is the hydraulic radius (m) and S_f is the friction slope.

Equation (1) can be used to calculate uniform flow in which the water-surface profile and energy gradient are parallel to the riverbed, and the river cross-section area, hydraulic radius and depth remain constant throughout the river reach (Jarrett 1985).

Considering uncertainties, Cowan (1956) proposed a formula using five parameters ($n = (n_b + n_1 + n_2 + n_3 + n_4)\cdot m$) to represent the influence of different variable factors, where n_b is a base value of n for a straight, uniform, smooth channel in natural materials; n_1 is a correction factor for the effect of surface irregularities; n_2 corrects for variations in the shape and size of the channel cross section; n_3 corrects for obstructions; n_4 corrects for vegetation and flow conditions; and m is a correction factor for meandering. Petryk & Bosmajian (1975) developed a method to derive n based on the vegetation density for a densely vegetated flood plain. The vegetation density has a strong impact on the roughness of a channel (Li *et al.* 2014). An equation was derived that incorporates the influence of the stem density on the flow resistance (Noarayanan *et al.* 2012); it was found that the energy loss of the head due to friction is caused by both vegetation and the side walls. Water flows through different river cross sections with different hydraulic radiuses. When the water depth is far less than the water flow width, the hydraulic radius is approximately equal to the water depth. Thus, n varies dynamically with the streamflow and changes in water depth. The value of n decreases with increasing depth of flow and varies directly with slope for high-gradient streams (Azamathulla & Jarrett 2013). However, the water depth is difficult to measure for all cross sections in an entire basin. Some equations for calculating n are based on an analytical model and solved by iteration (Li & Zhang 2001). The characteristic size of streambed particles has an influence on the roughness. Some studies investigated the relationships between the distribution of the particle sizes and n (Limerinos 1970).

The roughness coefficient is not a constant because the water depth and vegetation density change during different seasons in a basin. However, current hydrological models often apply a static n in calculations, without considering its dynamic changes. The roughness coefficient is a sensitive parameter in hydrological models (Ye *et al.* 2013). By contrast, some studies considered it to be an empirical parameter and calibrated the hydrological model by modifying the n value until the simulated discharge reasonably matched the observation (Mahmoudi *et al.* 2015). The n value based on more physical mechanisms can decrease the model uncertainty and parameter sensitivity (Aronica *et al.* 1998). There are obvious errors in the simulation for sub-basins, although the discharge simulation is satisfactory in large basin outlets because of equifinality for different parameters sets (Beven 2006). To simulate a flash flood or low flow and avoid parameter over-optimization in each sub-basin, dynamic roughness coefficient estimation (high-accuracy n) is absolutely necessary even for a large scale basin.

To manage the n value over a relatively accurate range, some studies have divided river cross sections into different strips with uniform roughness coefficients based on the land cover classification, which were from aerial photos and field surveys, to calibrate the n value by comparison with the observed water levels (Kovacs *et al.* 2006; Tóth 2009; Gichamo *et al.* 2012).

In this study, we tried to propose dynamic Manning's roughness coefficients (DMRC) and improve the routing of a hydrological model in basins.

The structure of the paper is as follows: immediately below the hydrological model and statistical method are described; a section introducing the data and study domain follows; next, a section presents the results and discussion; and the final section provides the conclusions.

METHOD DESCRIPTION

A new equation is proposed to simulate n using statistical analysis of the estimated n values from Manning's formula (Equation (1)) combined with the LAI, soil components, water depth and water surface width of a river. The new equation was then applied to improve the routing module of the Distributed Time-Variant Gain Hydrological Model (DTVGM) (Xia *et al.* 2005) (Figure 1). The DTVGM inputs are the precipitation, temperature and types of vegetation. The DTVGM outputs are discharge and evapotranspiration in sub-basins. The DMRC model is a

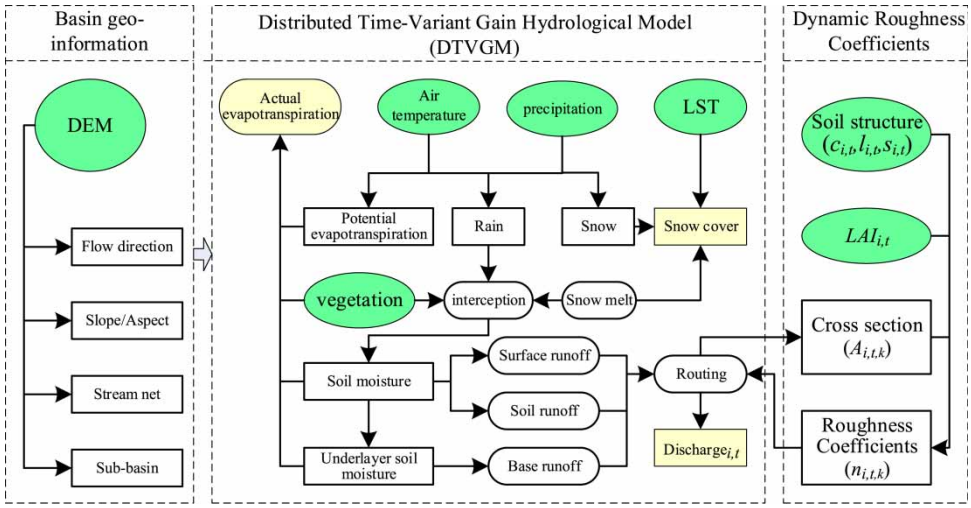

Figure 1 | The framework of dynamic roughness coefficients in the Distributed Time-Variant Gain Hydrological Model (DTVGM). LST is the land surface temperature; *c*, *l* and *s* are the clay, loam and sand percentages in soil, respectively; *LAI* is the leaf area index; *i* is the sub-basin number; *k* is the time step of iteration and *t* is the time.

module of DTVGM. The DMRC output is the roughness coefficient in the sub-basins. The DMRC inputs are the LAI, soil structure and water flow cross-section area (m^2), which is from the routing model output. The modelling time step occurs daily.

Distributed time-variant gain hydrological model

The DTVGM is a daily distributed hydrological model that incorporates runoff and routing modules. Coupling the advantages of both nonlinear and distributed hydrological models, the DTVGM can simulate variable hydrological processes under complex environmental conditions. It has been applied to two different cases: the Heihe River basin, which is in the arid and semi-arid region of north-western China; and the Chaobai River basin, which is in the semi-humid region of northern China (Xia *et al.* 2005). Multiple versions of the DTVGM have been proposed, and the model still undergoes continuous improvement and innovation.

Runoff module

The runoff module in DTVGM is based on the water balance principle by calculating evaporation, soil moisture, surface runoff, sub-surface runoff and base flow. The water balance equation is given as (Mao *et al.* 2016):

$$P_i = AW_{i+1} - AW_i + g_1 \cdot \left(\frac{AW_{ui}}{WM_u \cdot C_j}\right)^{g_2} \cdot P_i + AW_{ui} \cdot K_r + Ep_i \cdot \frac{AW_{ui}}{WM_u \cdot C_j} + AW_{gi} \cdot K_g \quad (2)$$

where P is the precipitation (mm), AW is the soil moisture (mm), AW_u is the upper soil moisture for a sub-basin (mm) (the subscript u means upper soil), AW_g is the lower soil moisture for a sub-basin (mm), WM_u is the upper field capacity (mm), Ep is the potential evapotranspiration, g_1 and g_2 are parameters ($0 < g_1 < 1$, $0 < g_2$) where g_1 is the runoff coefficient when soil is saturated and g_2 is a parameter for soil water, C is a land cover parameter, which ranges between 0.1 and 1. The value of C can be calibrated by observed data or experiment. K_r is the sub-surface runoff coefficient, K_g is the groundwater runoff coefficient, j is the sub-basin number and i is the period of time.

Routing module

The kinematic wave model is used in the routing module of DTVGM (Ye *et al.* 2013). The kinematic wave model simplifies the full de Saint Venant equations, where the friction term in the momentum equation is ignored. Therefore, it assumes that the friction and gravity forces balance each

other (Singh 1996). Assuming that the friction slope (S_f) is equal to the slope (S_0) and the river flow unsteadily varied in open channels (Ye *et al.* 2006a), the continuity equation can be written as:

$$\partial A/\partial t + \partial Q/\partial x = q \tag{3}$$

where A is the water flow cross-sectional area (m^2), t is the time (s), Q is the discharge (m^3/s), x is the flow path (m) and q is the lateral inflow (m^2/s).

The discharge at the water flow cross section is calculated based on Manning's formula and is shown below (Ye *et al.* 2013):

$$Q = A \cdot R^{2/3} \cdot S_f^{1/2}/n \tag{4}$$

where Q is the discharge of the flow (m^3/s), R is the hydraulic radius and A is the water flow cross-section area (m^2).

The n coefficient is often a constant in traditional hydrological models and land surface models. However, the most optimal n for a model is not always equal to a constant, it changes dynamically with the changing water flow cross-section area and vegetation in improved hydrological models.

It is assumed that the cross-sectional average width and water depth are linearly dependent in channels (Coe *et al.* 2008; Paiva *et al.* 2011) and the slope is a very wide and shallow river, the cross-sectional width w is equal to the river length L, w = L (m) in the slope (Ye *et al.* 2013):

$$w = 2ah \Rightarrow A = \frac{w \cdot h}{2} = ah^2 \Rightarrow h = \left(\frac{A}{a}\right)^{1/2} \tag{5}$$

where h is the average water depth (m), w is the average water width (m) and a is a parameter determined by river attributes.

The discharge from the cross section can be computed as:

$$\begin{aligned} Q &= \frac{1}{n} A \cdot R^{2/3} \cdot S_f^{1/2} = \frac{1}{n} A \cdot \left(\frac{A}{2h\sqrt{1+a^2}}\right)^{2/3} \cdot S_f^{1/2} \\ &= \frac{1}{n} \cdot S_0^{1/2} \cdot A \cdot \left(\frac{aA}{4a^2+4}\right)^{1/3} \\ &= \frac{1}{n} \cdot S_0^{1/2} \cdot (4a^2+4)^{-1/3} \cdot a^{1/3} \cdot A^{4/3} \end{aligned} \tag{6}$$

By setting $\alpha = (1/n) \cdot S_0^{1/2} \cdot (4a^2+4)^{-1/3} \cdot a^{1/3}$, $\beta = 4/3$, S_0 is the river bed slope (assuming that the friction slope S_f is equal to the slope S_0 in order to simplify the model), the flow route length (Δx) is equal to the river length: $\Delta x = L$, the large Δx may incur error in the application and dividing the river length into some segments can decrease the error, the inflow term q is equal to the lateral flow term Q_s/L, Q_s is the discharge ($m^3 \cdot s^{-1}$) from the slope to the river of the sub-basin (the slope area is small, Q_s is equal to runoff, or Q_s can be calculated by slope routing model), and the finite difference representation of equation $(\partial A/\partial t) + (\partial Q/\partial x) = q$ is:

$$\Delta A L + \Delta Q \Delta t = Q_s \Delta t \tag{7}$$

Denoting $\Delta A = A_t - A_{t-1}$ at t time and $\Delta Q = Q_O - Q_I$, where A is the water flow cross-sectional area (m^2), Q_I is the input discharge ($m^3 \cdot s^{-1}$), Q_O is the output discharge ($m^3 \cdot s^{-1}$), and can be calculated as:

$$Q_O = \alpha \cdot \left(\frac{A_t + A_{t-1}}{2}\right)^{\beta} \tag{8}$$

Combining Equations (6) and (7) with (8), we obtain:

$$A_t - A_{t-1} = \left(Q_I - \alpha \cdot \left(\frac{A_t + A_{t-1}}{2}\right)^{\beta}\right) \frac{\Delta t}{L} + \frac{Q_s \Delta t}{L} \tag{9}$$

If we set

$$f(A_t) = \left(Q_I - \alpha \cdot \left(\frac{A_t + A_{t-1}}{2}\right)^{\beta}\right) \frac{\Delta t}{L} + \frac{Q_s \Delta t}{L} - A_t + A_{t-1} \tag{10}$$

$$f'(A_t) = -\frac{\alpha\beta}{2} \cdot \left(\frac{A_t + A_{t-1}}{2}\right)^{\beta-1} \frac{\Delta t}{L} - 1 \tag{11}$$

$$A_t^{(k)} = A_t^{(k-1)} - \frac{f(A_t^{(k-1)})}{f'(A_t^{(k-1)})} \tag{12}$$

where k is the time step of iteration.

Statistical analysis method

In prior research, the n value in Manning's formula was a function of the vegetation density, soil components, water depth and surface width of rivers (Moharana & Khatua 2014). In this study, we analysed the relationships between n and the water depth and surface width using linear regression. An optimal equation for calculating n was then derived based on multiple nonlinear regression.

Multiple regression analysis is an appropriate method when the research problem includes one unique metric-dependent variable and a dependent-variable that is related to more than one metric-independent variable (Hair *et al.* 2006). The general purpose of multiple regression analysis is to learn about the relationship between several independent or predictive variables and a dependent or criterion variable (Enayatollahi *et al.* 2014). Additionally, an advantage of multiple nonlinear regression is that a very high order multivariate should be able to approximate complex multivariate functions (Cogger 2010).

Experimental results have indicated that Manning's roughness coefficient n increases with the increasing vegetation density, which leads to higher flow resistance in natural channels and hillsides (Li *et al.* 2014). The vegetation density is difficult to obtain in basins. However, the leaf area index (LAI) can be measured by remote sensing. Instead of the vegetation density, the LAI was used in this study to develop a formula for calculating the n. In the simulation process, the LAI was set to $(LAI + 1)$ to avoid calculation errors when the LAI equals zero in bare areas.

Stream bed roughness is associated with bed material, especially the particle size and distribution (Limerinos 1970). We selected a soil particle (clay, loam and sand content) dataset for the bed material information.

The final formula is as follows:

$$n = p_1(c + 2 \cdot l + 3 \cdot s)(LAI + 1)^{p_2} A^{p_3} / \sqrt{2g} \quad (13)$$

where c, l and s are the clay, loam and sand percentages in soil, respectively; LAI is leaf area index; A is the water flow cross-section area (m^2); g is the gravitational acceleration; and p_1, p_2 and p_3 are parameters. The roughness of the flood plain is higher than the roughness in the river because the river bed was washed clean with water; then, the p_1 of the flood plain was set to greater than the p_1 in the river when it was used in the hydrological model. p_2 can indicate the sensitivity of vegetation. The large p_2 shows that vegetation is sensitive to roughness. p_3 indicates that the cross sections are large or small or have sharp bends, constrictions, or side-to-side shifting of the low-water channel.

Equation (13) was used in the routing process in an entire basin; n was separately calculated in each sub-basin during each time period. The water flow cross-sectional area can be computed using Newton iterations (Equation (12)) in both channels and slopes. A continuous and consistent LAI (Yuan *et al.* 2011) is composited every 8 days at 1-km resolution. The LAI was interpolated into the sub-basins. The LAI in the channels and slopes are equal to the LAI that locates in sub-basins. The A and LAI vary across time and space.

The p_1, p_2 and p_3 parameters were optimized by 1stOpt (http://www.7d-soft.com/). 1stOpt is a robust, easy-to-use and powerful optimization tool that is widely used in various engineering fields. Based on the optimization software package 1stOpt, multiple nonlinear regression can be easily established and solved (Wang *et al.* 2009; Hu *et al.* 2011). The 1stOpt search of optimization capability is stronger than that of other simulation software because it can find relatively accurate results from any initial value (Tang *et al.* 2008). The Levenberg–Marquardt + Universal Global Optimization of 1stOpt was applied to optimize a set of parameters in Equation (2).

There are three steps to calculate dynamic n: 1) reading the soil structure and LAI at t time, 2) deriving the water flow cross-sectional area using Newton iterations (Equation (13)) based on $n_{t,k-1}$, 3) using Equation (2) to calculate $n_{t,k}$ for the next iteration. Therefore, n is dynamic in the improved routing module.

Model performance measures

To evaluate the effectiveness of the simulation, the following four statistical indices are used: the relative Bias (*rBias*), correlation coefficient (R), Nash–Sutcliffe efficiency value (*NSE*) and root-mean-square-error (*RMSE*). They are

evaluated by:

$$rBias = \frac{\overline{Q_c} - \overline{Q_0}}{\overline{Q_0}} * 100\% \quad (14)$$

$$NSE = \left[1 - \frac{\sum_{i=1}^{m} (Q_{c,i} - Q_{0,i})^2}{\sum_{i=1}^{m} (Q_{o,i} - \overline{Q_0})^2}\right] * 100\% \quad (15)$$

$$R = \frac{\sum_{i=1}^{m} (Q_{c,i} - \overline{Q_c})(Q_{o,i} - \overline{Q_0})}{\sqrt{\sum_{i=1}^{m} (Q_{c,i} - \overline{Q_c})^2 \cdot \sum_{i=1}^{m} (Q_{o,i} - \overline{Q_0})^2}} \quad (16)$$

and

$$RMSE = \sqrt{\sum_{i=1}^{m} (Q_c - Q_0)^2 / m} \quad (17)$$

where Q_0, Q_c, $\overline{Q_0}$ and $\overline{Q_c}$ are the observed flow, simulated flow, average observed flow and average simulated flow, respectively. m is the number of simulation and observation pairs.

rBias refers to the correspondence between the average simulated value and the average observations. *R* checks the fitness of the simulated and observed values. The *RMSE* is used to measure the deviation between the observation and simulated values. If *NSE* is close to 1, the model is considered to have good quality and be highly reliable. If it is close to 0, the simulation is close to the observed value of an average level and the overall results are legitimate, but a bad simulation error has occurred. If the *NSE* is smaller than 0, the model is not reliable.

DATA AND STUDY DOMAIN

The Yellow River is the second-longest river (Figure 2) in China, originating from the Tibetan plateau. It passes through the northern semi-arid region, crosses the Loess Plateau and finally discharges into the Bohai Gulf (Yang *et al.*

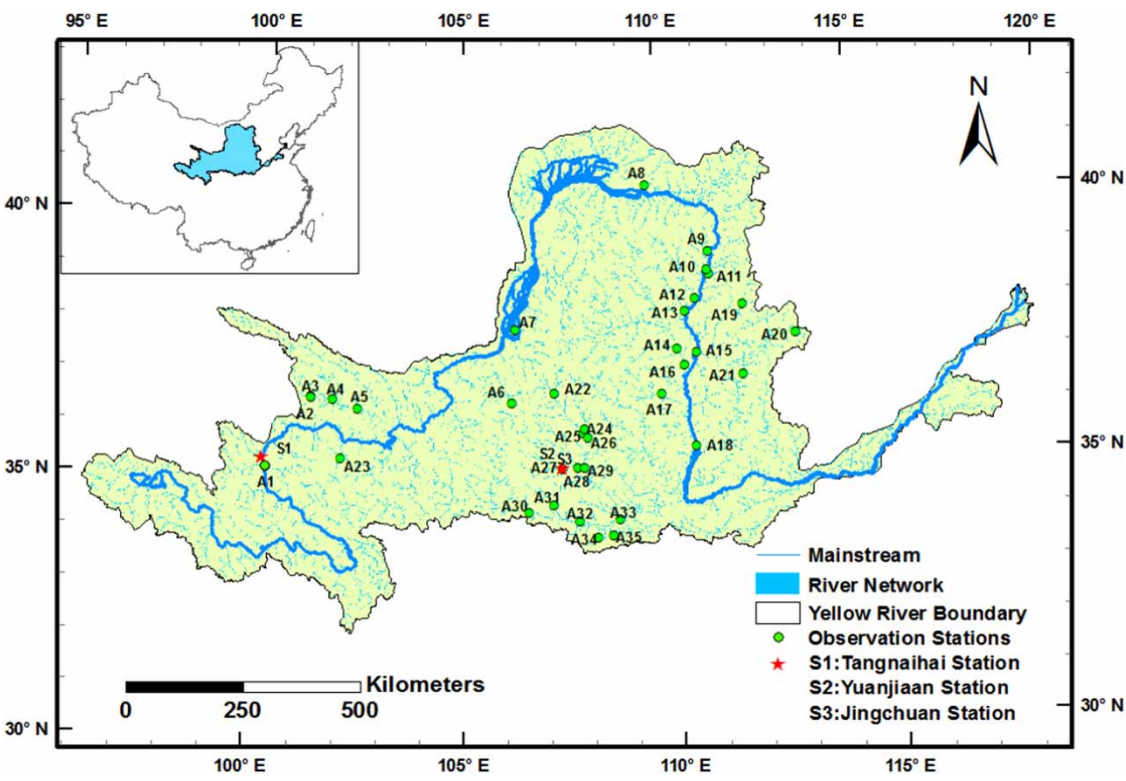

Figure 2 | Location of hydrological stations in the Yellow River basin.

2004). The main course of the Yellow River flows for approximately 5,464 km and has a drainage basin area of approximately 752,443 km^2. The Yellow River was divided into 3,316 sub-basins, and each sub-basin area is greater than 100 km^2. The climate conditions vary from cold to temperate zones and change from arid and semi-arid to semi-humid regions (Cheng 1996). The annual precipitation for the Yellow River is approximately 450 mm. However, the annual evaporation is 1,100 mm.

There are 35 stations with estimated data to simulate the roughness coefficient (Table 1), which include the water surface width (w), discharge (Q), water depth (H), friction slope (s) and roughness coefficients (n) for the period from 2008 to 2012, obtained from hydrological year books of the Yellow River Basin. The Manning's roughness coefficient is estimated using Manning's formula.

The observed discharge in three hydrological stations was selected to compare the raw (the model with static n) and improved (the model with dynamic n) model results. We selected the three stations because it is very difficult to obtain more observed discharge data in other small catchments. Tangnaihai station has a 121,927 km^2 drainage area in the upper Yellow River basin; Jingchuan and Yuanjiaan stations have 3,145 km^2 and 1,661 km^2 drainage areas, respectively, in the midstream Yellow River basin. Additionally, the observed daily discharge data (from 1998 to 1999) of Tangnaihai station, Yuanjiaan station and Jingchuan station were collected from the Yellow River Conservancy Commission (YRCC).

Daily precipitation and potential evaporation data from 1955 to 2012 were provided by the China Meteorological Administration. There are 983 precipitation gauges and 839 evaporation gauges in continental China. A continuous and consistent LAI (Yuan *et al.* 2011) is composited every 8 days at 1-km resolution, and a conterminous China multi-layer soil particle-distribution dataset (clay, loam and sand content) was developed by Shangguan *et al.* (2012) with a resolution of 1 km × 1 km.

The daily precipitation and evaporation data, LAI (Figure 3) and Yellow River soil particle-distribution (Figure 4) were interpolated into the 3,316 sub-basins. Figure 3 shows that the LAI on the slope is much larger than that from the main streams. The LAI value is much larger in the upstream and downstream in July. The main

Table 1 | Hydrological station information

ID	Station name	Longitude	Latitude	Annual streamflow (m^3/s)
A1	Damitan	100.24	35.32	19
A2	Huangyuan	101.27	36.68	7.32
A3	Dongjiazhuang	101.27	36.67	2.13
A4	Xining	101.78	36.63	18.2
A5	Ledu	102.41	36.48	39.6
A6	Hanfuwan	106.15	36.60	0.331
A7	Guojiaqiao	106.25	37.98	3.64
A8	Hademengou	109.63	40.68	0.006
A9	Hequ	111.15	39.37	474
A10	Fugu	111.08	39.03	500
A11	Qiaotou	111.13	38.93	0.01
A12	Wenjiachuan	110.75	38.48	4.75
A13	Gaojiachuan	110.48	38.25	6.32
A14	Dingjiagou	110.25	37.55	18.3
A15	Wubao	110.72	37.45	562
A16	Baijiachuan	110.42	37.23	19.6
A17	Ganguyi	109.80	36.70	3.36
A18	Longmen	110.58	35.67	562
A19	Jingle	111.92	38.33	10.8
A20	Dudui	113.18	37.72	0.846
A21	Yitang	111.83	37.00	10.5
A22	Hongde	107.19	36.76	1.33
A23	Tongren	102.02	35.52	15.1
A24	Jiaqiao	107.90	36.08	2.37
A25	Qingyang	107.88	36.00	3.99
A26	Banqiao	107.98	35.92	0.386
A27	Jingchuan	107.35	35.33	2.58
A28	Yangjiaping	107.74	35.33	8.95
A29	Yuluoping	107.89	35.33	8.69
A30	Tuoshi	106.53	34.49	27.1
A31	Qianyang	107.13	34.63	4.46
A32	Weijiabao	107.74	34.30	33.6
A33	Xianyang	108.70	34.32	62
A34	Laoyukou	108.53	34.02	2.94
A35	Chenhe	108.16	33.98	7.4
S1	Tangnaihai	130.37	46.82	630
S2	Yuanjiaan	107.3524	35.3355	2.1
S3	Jingchuan	107.3523	35.3398	4.98

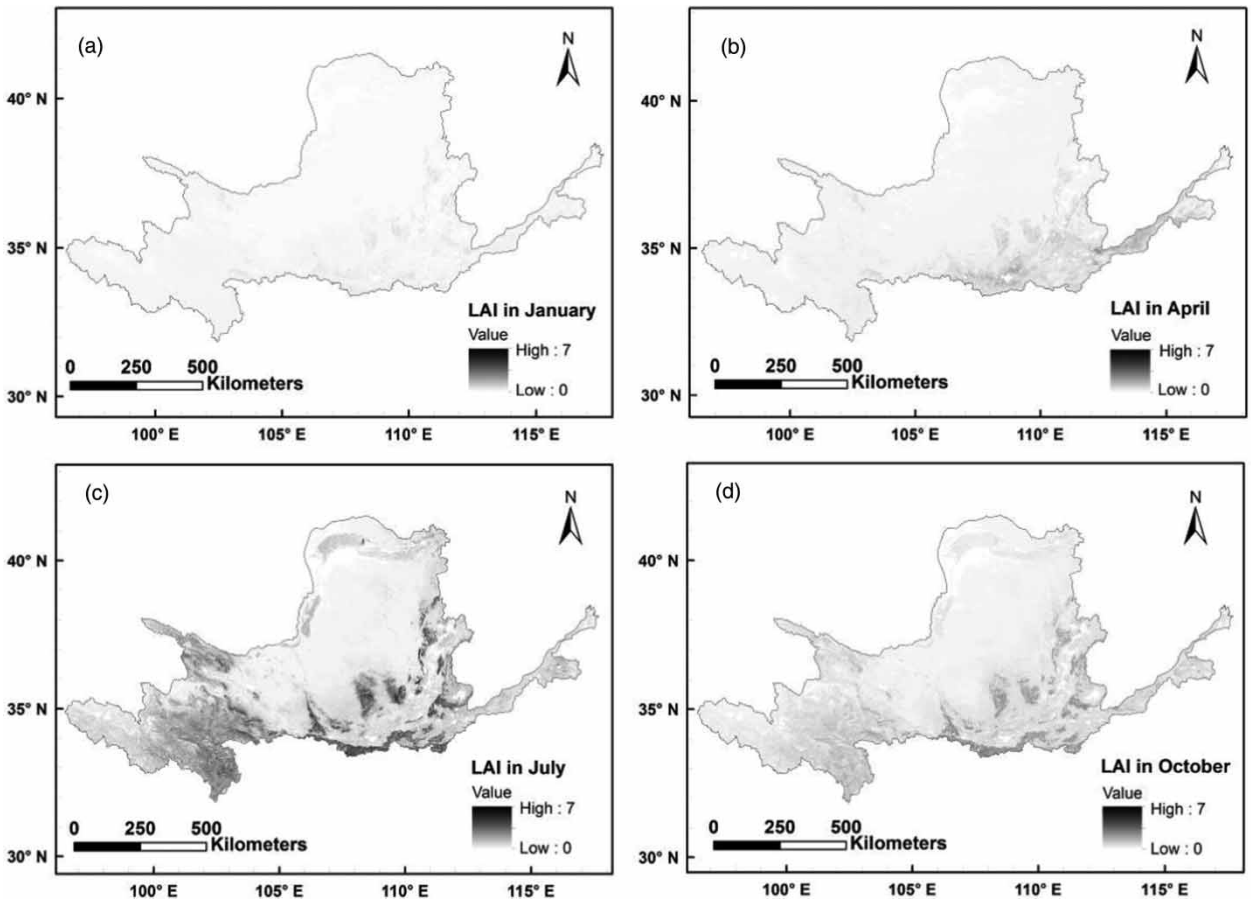

Figure 3 | The mean spatial distribution of LAI in (a) January, (b) April, (c) July and (d) October in the Yellow River basin.

causes are that approximately 70% of the total annual rainfall is restricted to the summer (June–September) (Ye *et al.* 2006b), and there is a desert in the middle stream in the Yellow River basin.

RESULTS AND DISCUSSION

Statistical analysis of estimated *n* with each of the components

From the definition of the roughness coefficient, we know that the roughness coefficients were determined by the soil, specific discharge conditions, and size, shape and types of vegetation that line the bed and sides of the channel. Therefore, we selected the composition of the soil (sand, loam and clay), LAI and water flow cross-section area to estimate the n value. We collected 1,177 estimated roughness coefficients and corresponding water depths, surface widths, LAIs and soil data from 35 hydrostations. However, the samples were not sufficient to quantify the effect of soil and vegetation in 35 stations. Li (2014) and Noarayanan *et al.* (2012) studied vegetation–flow interactions under laboratory conditions. Their study showed that the Manning's vegetation roughness coefficient due to vegetation resistance increased with the increasing vegetation density. We used their results in our study. The roughness coefficient is closely related to the particle size and distribution (Limerinos 1970). Limerinos (1970) reported that the large particle size increased the roughness coefficient by using 11 catchment data sites in the USA.

To explore the relationship between the n value and water depth d and surface width w, scatter diagrams were produced to support the statistical analysis.

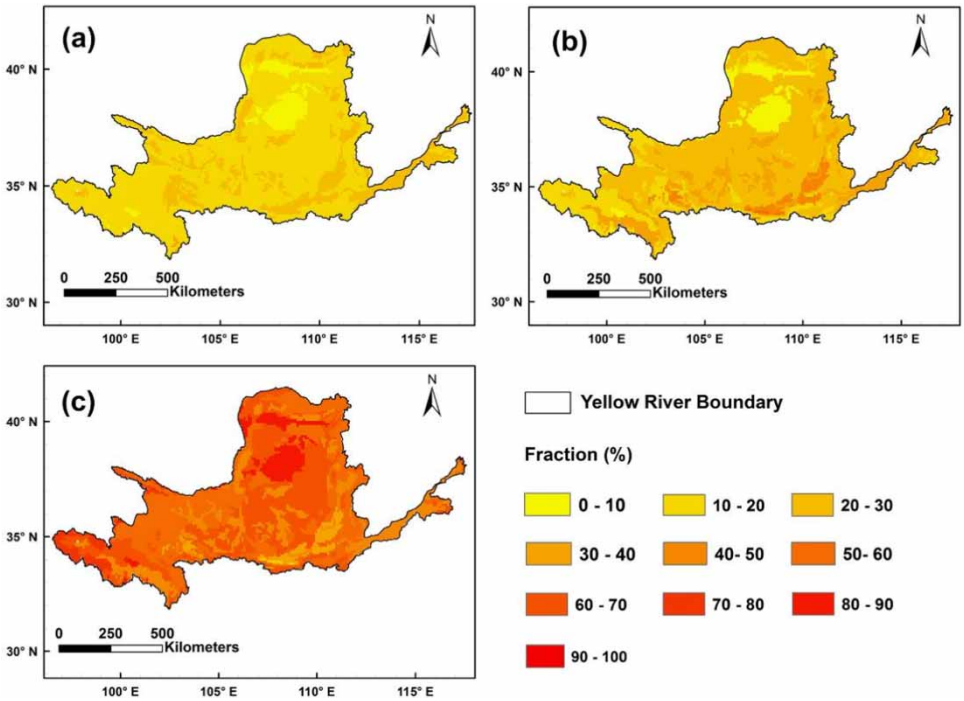

Figure 4 | Clay, loam and sand fractions in the Yellow River: (a) clay fraction, (b) loam fraction and (c) sand fraction (Shangguan *et al.* 2012).

The observed d and estimated n values for six stations are shown in Figure 5. Obviously, there is a negative relationship between d and n for the Tongren, Huangyuan, Xining, Ledu and Dongjiazhuang stations, meaning that Manning's n decreases with an increase of water depth. This means that less energy was consumed as the flow depth increased in open channels. This behaviour was also confirmed by Fippin-Dudley *et al.* (1998). However, this negative relationship is not shown for Damitan station. The main cause is that a decreasing n value is a comprehensive function of multiple factors, such as the riverbed irregularity, vegetation density and particle sizes in a riverbed. The riverbed has been cleared and fixed at Damitan station such that the roughness is more like constant at Damitan station.

Figure 6 shows the variation of n with the water surface width. The n value decreases with increasing water surface width, meaning that broader water surface width will generate lower flow resistance.

Roughness coefficient model calibration and validation

The hydrological stations shown in Figure 2 are labelled, starting from upstream of the Yellow River to the downstream. There are only 1,177 estimated n values by Manning's formula in 35 stations. The data period is from 2008 to 2012. The period is too short, and we wanted to verify the improved method in different locations. Therefore, the observed data of 21 stations (A1–A21) were used to calibrate the parameters in Equation (2), and the data from the remaining 14 stations (A22–A35) were used to validate the p_1–p_3 parameters.

The values for p_1, p_2 and p_3 of Equation (2) were 0.19 (0.475 in river), 0.2, and −0.15, respectively, according to the multiple nonlinear regression method. Equation (2) can be represented by Equation (11) with the substitution parameters.

$$n = 0.19*(c + 2l + 3s)(LAI + 1)^{0.2}A^{-0.15}/\sqrt{2g} \quad (18)$$

The results of the calibration and the validation period are shown in Figure 7. The correlation coefficient is 0.71 and the *RMSE* is 0.019 between the estimated and simulated n for the calibration (A1–A21). The correlation coefficient is 0.70 and the *RMSE* is 0.016 for the validation (A22–A35). The results showed that the formula of Equation (2) for calculating n is reliable and that the parameters (p_1, p_2 and p_3) are suitable for the Yellow River basin.

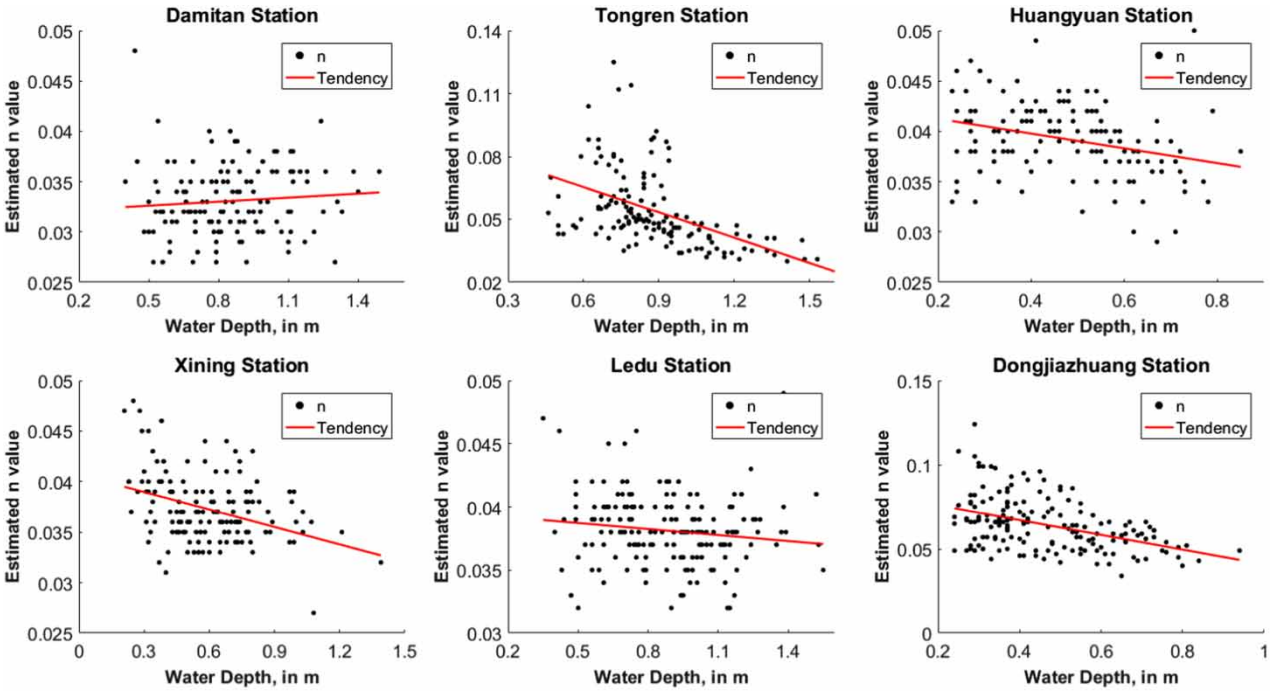

Figure 5 | Relationship between the estimated *n* value and water depth (*d*).

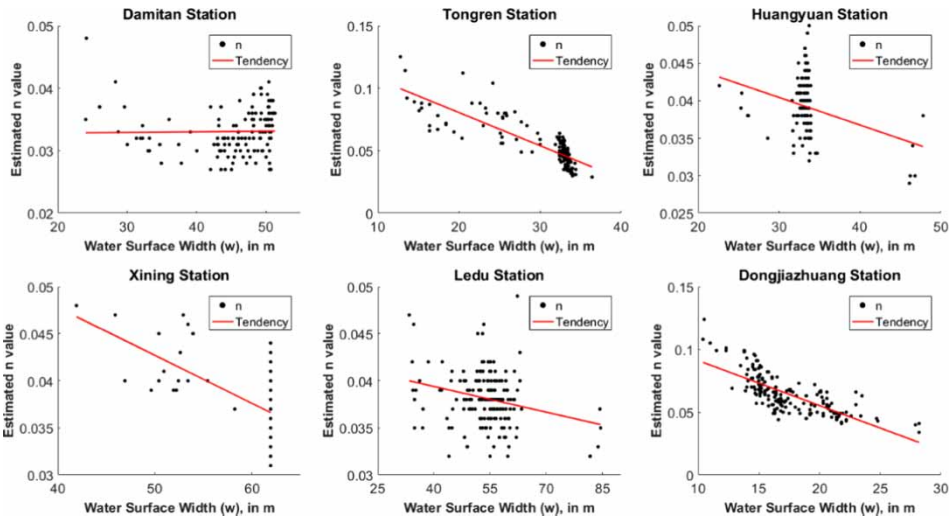

Figure 6 | Relationship between the estimated *n* value and surface water width (*w*).

There are different percentages of clay, loam and sand in each type of soil. With a large particle size, *n* is large in sand. Furthermore, a high vegetation density contributes to the resistance of flow.

Validation of roughness coefficient in the DTVGM

In the DTVGM, each sub-basin is defined as a hydrological unit to calculate the runoff, roughness coefficients and routing.

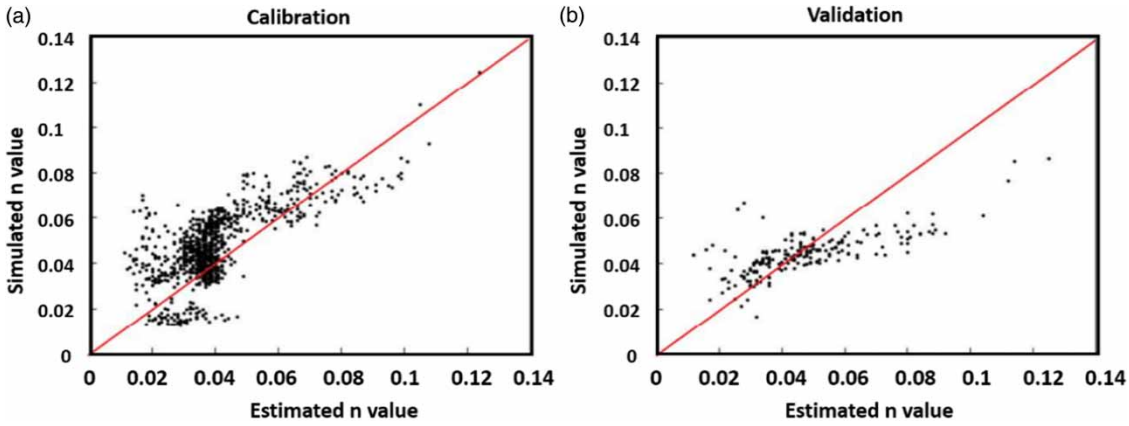

Figure 7 | Relationship between the simulated *n* and estimated *n* in (a) the calibration period and (b) the validation period.

Table 2 shows the DTVGM parameter values. These parameters were the optimized results from using the observed streamflow. A manual calibration method was used to calibrate the model parameters because the distributed hydrological model takes a long time to run, and automatic calibration would be too time-consuming. During manual calibration, the model was run a few times to ensure that *NSE*, *R* and *rBias* were good. Due to the difference of vegetation, soil and climate between upstream and downstream in the Yellow River basin, the parameters of the runoff module are different at different hydro-stations.

Except for the roughness coefficients, parameters in the raw (static *n*) DTVGM and improved (dynamic *n*) DTVGM are the same at the same station. Using the raw and improved DTVGM, we produced raw and improved simulated discharges.

Figures 8–10 show the daily hydrograph of Tangnaihai, Jingchuan and Yuanjiaan stations in 1998 and 1999. In Figure 8(a), the two lines of the raw discharge and improved discharge are almost the same and the difference of error is not obvious, mainly because Tangnaihai station is located in the main channel of the Yellow River, and the catchment area is very large (121,972 km^2). The Manning's n is greater than true value in main river channels and less than true value in the slopes in the static Manning's n model. The velocity of the flow would decrease if *n* increases and other conditions do not change, and vice versa. The Manning's *n* is not equal to true value in slopes and river channels, the simulated velocity of the flow is smaller than true value in slopes and is greater than true value in river channels. The total simulated streamflows are similar because the errors are offset in slopes and river channels. Figure 8(b) depicts the absolute error between the observed and simulated discharge. However, the absolute error in Figures 9(b) and 10(b) is more obviously different than that in Figure 8(b). The drainage areas of the Jingchuan and Yuanjiaan catchments are small. The simulated flood peak in the improved model is less than that in the raw model and is more close to the observed discharge in Figures 9(a) and 10(a). The improved model affords a reasonable roughness to the slope, making the new simulated discharge more accurate than the raw simulated discharge in a small catchment. This means that the improved model can increase the flood simulation accuracy on the slope by affording an accurate roughness on the slope.

Table 2 | Parameters of the DTVGM

Station	g_1	g_2	K_r	K_g	n	p_1 (slope)	p_1 (river)	p_2	p_3
Tangnaihai	0.4	1	0.1	3	0.04	0.15	0.375	0.2	−0.25
Jingchuan	0.35	1.6	0.1	2	0.04	0.15	0.375	0.2	−0.25
Yuanjiaan	0.3	2	0.1	2	0.04	0.15	0.375	0.2	−0.25

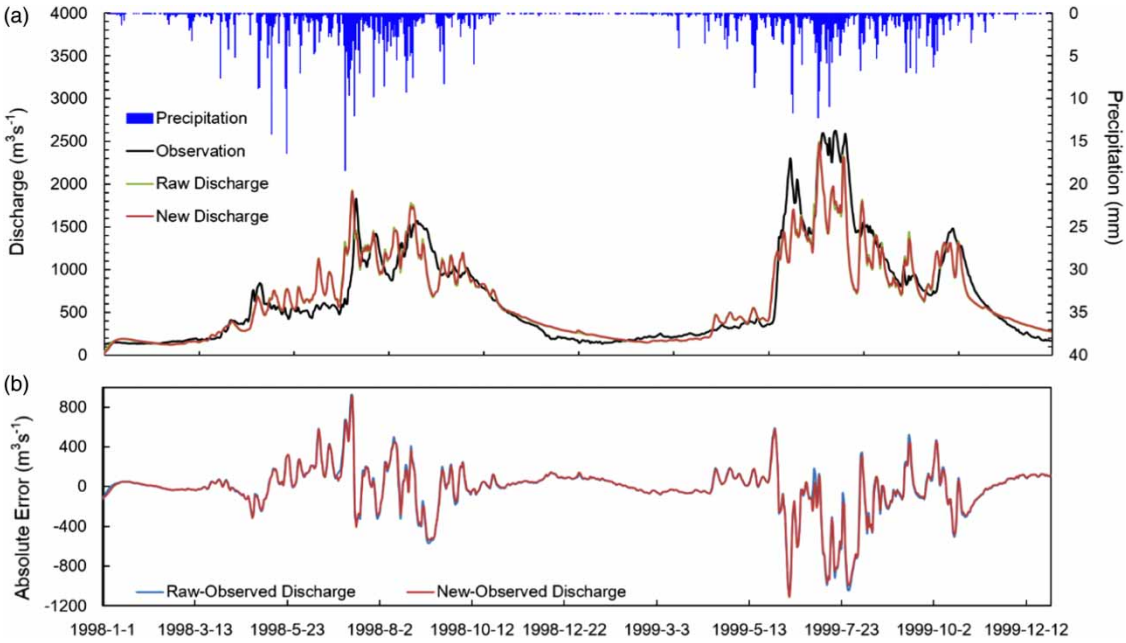

Figure 8 | The daily hydrograph (a) and absolute error (b) in 1998 and 1999 at Tangnaihai station. The raw-observed discharge is the raw model simulated discharge minus the observed discharge. The improved-observed discharge is the new model simulated discharge minus the observed discharge.

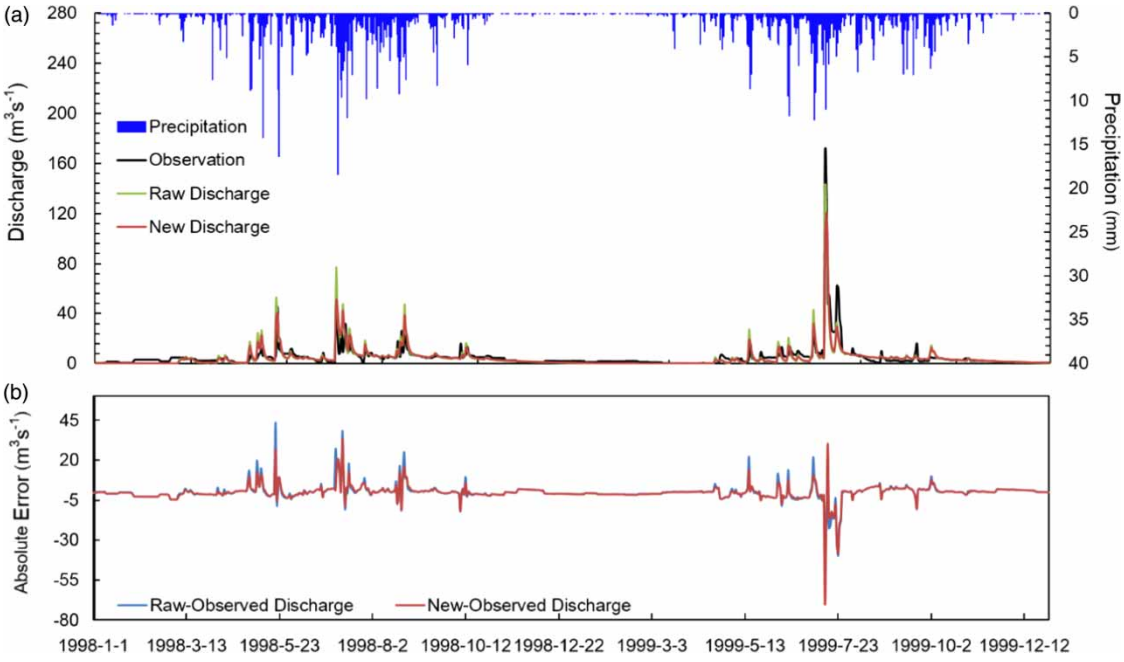

Figure 9 | The daily hydrograph (a) and absolute error (b) in 1998 and 1999 at Jingchuan station. The raw-observed discharge is the raw model simulated discharge minus the observed discharge. The improved-observed discharge is the new model simulated discharge minus the observed discharge.

The improved and raw model performance indices are shown in Table 3. The indices show that the improved model performs better than the raw model. The indices did not markedly increase in the large basin, but they obviously increased in a small catchment.

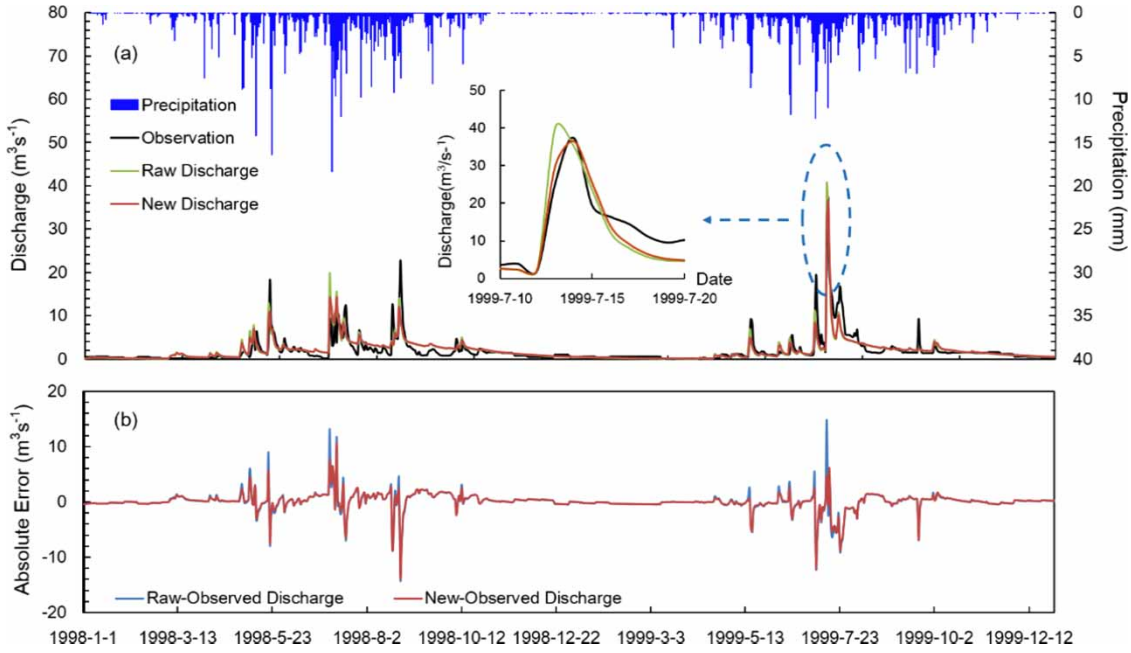

Figure 10 | Raw and improved simulated discharges at Yuanjiaan station.

Table 3 | Model performance indices in the Yellow River basin

			NSE		*R*		*rBias (%)*	
Station	**No.**	**Drainage area (km²)**	**Raw**	**Improved**	**Raw**	**Improved**	**Raw**	**Improved**
Tangnaihai	40100350	121,972	0.821	0.830	0.909	0.915	−2.3	−2.6
Jingchuan	41200500	3,145	0.742	0.751	0.865	0.867	−1.2	−2.5
Yuanjiaan	41202000	1,661	**0.656**	**0.736**	0.819	0.859	4.8	4.2

Tangnaihai station is a control station in the Yellow River source area, and Jingchuan and Yuanjiaan stations are located midstream. The data period is 1998–1999.

To clearly justify why having a dynamic Manning's roughness is necessary, the flood peak anomaly percentage (*FPAP*, %) was used to compare the simulated flood peak at sub-basins from the improved and the raw models:

$$FPAP = \frac{Q_{d\max} - Q_{s\max}}{Q_{s\max}} \cdot 100\% \quad (19)$$

where Q_{dmax} is the simulated flood peak with dynamic Manning's n (m^3/s), Q_{smax} is the simulated flood peak with static Manning's n (m^3/s), and all other data and parameters are the same in the improved and the raw models.

Figure 11 shows the spatial distributions of the flood peak anomaly percentage during 1998 to 1999 in the Yellow River basin. The *FPAP* is less than zero at the slope because the dynamic Manning's n is greater than the static Manning's n at the slope. However the *FPAP* is close to zero in the main river channel because the dynamic Manning's n is less than the static Manning's n in the river channel. The minimum *FPAP* is −45%, which shows that the simulated flood peak may have a large error at the slope with the static Manning's n, although the model has high performance at the basin outlet (Table 3).

The hourly flood peak is larger than the daily flood peak at the same time, and the hourly low flow is smaller than the daily low flow. The hourly n will be more variable than the daily n, resulting in a variable flow cross section (Equation (1)). Therefore, the hourly performance will be better than

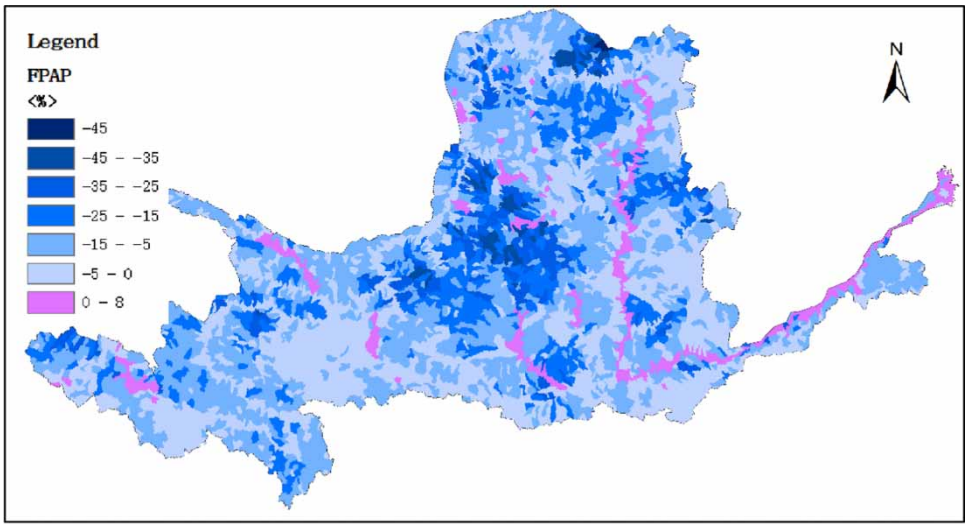

Figure 11 | Spatial distributions of the flood peak anomaly percentage (*FPAP*, %) during 1998 to 1999 in the Yellow River basin.

the daily performance using the dynamic *n* model. However, it is very difficult to obtain hourly discharge data over a long period. We will continue to study the hourly data in the future.

Figure 12 shows the seasonal spatial distribution of *n* in 1998 for the Yellow River. The *n* values were calculated by Equation (2) in the DTVGM. The *n* values are very small along the river channel and large on the slopes. The main causes are the higher vegetation density and shallower water depth on the slopes. The *n* values are small in spring and summer in the river channel because the water is deep during those two seasons. However, *n* is large in spring and summer on the slopes because the vegetation is luxuriant in spring and summer. The reverse result is shown in autumn and winter.

Strengths and weaknesses of dynamic *n* model

There are three advantages for applying the dynamic *n* in the hydrologic model. 1) The dynamic *n* is close to the true *n* value, and it is better than a constant in the raw hydrologic model. A more physical mechanistic parameter can decrease the model uncertainty and sensitivity of the parameter. 2) The improved simulated discharge will have a higher accuracy than the raw model in sub-basins. 3) The satisfactory spatial-temporal distribution of n can improve the flash flood and low flow simulations.

The weaknesses of the model are as follows: 1) the dynamic *n* equation is a statistic formula, making it difficult to calibrate the parameters and 2) higher resolution DEM, vegetation and soil structure datasets are needed to calculate the dynamic *n*.

CONCLUSIONS

This research proposed a new way to provide a dynamic spatial-temporal distribution of Manning's roughness coefficients for hydrological models in basins. Based on the new concept, a distributed hydrological model was improved and applied to the Yellow River in China. The results have already shown that the improved model can provide more accurate simulated streamflow than the raw model. The new scheme of *n* took the LAI, soil components, hydraulic radius and water flow cross-section area into consideration, producing new *n* values that are closer to the true values than those from the raw model, especially on slopes. The *n* values are very small along the river channel and large on the slopes. The simulated flood peak may have a large error at the slope with the static Manning's *n*, although the model has high performance at the basin outlet. The simulated streamflow with the dynamic Manning's *n* is more accurate than that with the static Manning's *n*. The dynamic spatial-temporal distribution of

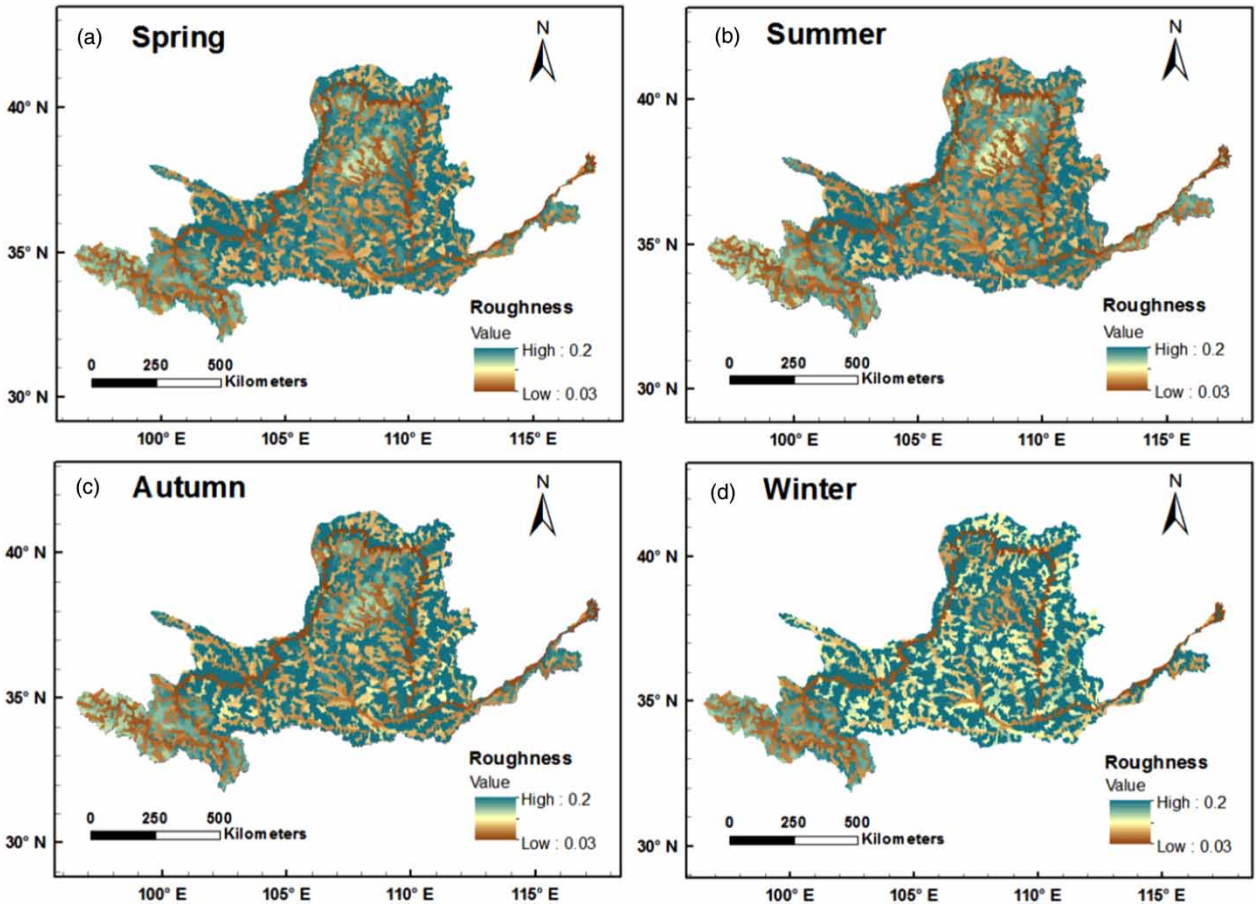

Figure 12 | The seasonal spatial distribution of the roughness coefficients in the Yellow River in 1998: (a) spring, (b) summer, (c) autumn, and (d) winter.

n can now be used in other hydrological models or land surface models.

In the future, we will keep working to improve the roughness coefficient equation based on higher resolution data and other observed information. Additionally, we will develop a global routing in the land surface model using the new *n* scheme.

ACKNOWLEDGEMENTS

This study was supported by the Natural Science Foundation of China (No. 41475093), the Intergovernmental Key International S&T Innovation Cooperation Program (No. 2016YFE0102400) and the State Key Laboratory of Earth Surface Processes and Resource Ecology Open Research Program (NO. 2017-KF-17).

REFERENCES

Arcement, G. J. & Schneider, V. R. 1989 Guide for selecting Manning's roughness coefficients for natural channels and flood plains. *United States Geological Survey Water-Supply Paper* **2339**, 1–38.

Aronica, G., Hankin, B. & Beven, K. 1998 Uncertainty and equifinality in calibrating distributed roughness coefficients in a flood propagation model with limited data. *Advances in Water Resources* **22**, 349–365.

Azamathulla, H. M. & Jarrett, R. D. 2013 Use of gene-expression programming to estimate Manning's roughness coefficient for high gradient streams. *Water Resources Management* **27**, 715–729.

Barling, R. D. & Moore, I. D. 1994 Role of buffer strips in management of waterway pollution: a review. *Environmental Management* **18** (4), 543–558.

Beven, K. 2006 A manifesto for the equifinality thesis. *Journal of Hydrology* **320**, 18–36.

Cheng, X. 1996 *Hydrology of the Yellow River Basin.* Yellow River Press, Zhengzhou (in Chinese).

Coe, M. T., Costa, M. H. & Howard, E. A. 2008 Simulating the surface waters of the Amazon River basin: impacts of new river geomorphic and flow parameterizations. *Hydrological Processes* **22**, 2542–2553.

Cogger, K. O. 2010 Nonlinear multiple regression methods: a survey and extensions. *Intelligent Systems in Accounting, Finance & Management* **17**, 19–39.

Coon, W. F. 1995 *Estimates of Roughness Coefficients for Selected Natural Stream Channels with Vegetated Banks in New York.* Report, U.S. Geological Survey, New York, pp. 93–161.

Cowan, W. L. 1956 Estimating hydraulic roughness coefficients. *Agricultural Engineering* **37**, 473–475.

Enayatollahi, I., Bazzazi, A. A. & Asadi, A. 2014 Comparison between neural networks and multiple regression analysis to predict rock fragmentation in open-pit mines. *Rock Mechanics and Rock Engineering* **47**, 799–807.

Fippin-Dudley, S. J., Abt, S. R., Bonham, C. D., Watson, C. C. & Fischenich, J. C. 1998 *Evaluation of Flow-Resistance Equations for Vegetated Channels and Floodplains.* Report, U.S. Army Engineer Research and Development Center, Vicksburg, Mississippi.

Gichamo, T. Z., Popescu, I., Jonoski, A. & Solomatine, D. 2012 River cross-section extraction from the ASTER global DEM for flood modeling. *Environmental Modelling & Software* **31**, 37–46.

Hair, J. F., Black, W. C., Babin, B. J., Anderson, R. E. & Tatham, R. L. 2006 *Multivariate Data Analysis.* Prentice Hall International, Madrid.

Hu, S., Cheng, X., Chai, F., Gao, J. & Yang, G. 2011 Optimal regulation model of reservoir discharge based on 1 stopt. *Journal of Hohai University: Natural Sciences* **39**, 377–383.

Jarrett, R. D. 1985 *Determination of Roughness Coefficients for Streams in Colorado.* Report, Water Resources Invest, Lakewood, Colorado, 85-4004.

Jochen, S., Evzen, Z. & Jiri, M. 2006 *Flood Risk Management: Hazards, Vulnerability and Mitigation Measures.* Springer, Dordrecht.

Kovacs, S., Kiss, A. & Szekeres, J. 2006 Experiences in application of HEC-RAS model under circumstances of flood waves. In: *Flood Risk Management: Hazards, Vulnerability and Mitigation Measures (*J. Schanze, E. Zeman & J. Marsalek, eds). Springer, Dordrecht, pp. 47–58.

Kumar, D. N., Baliarsingh, F. & Raju, K. S. 2011 Extended Muskingum method for flood routing. *Journal of Hydro-Environment Research* **5**, 127–135.

Li, Z. & Zhang, J. 2001 Calculation of field Manning's roughness coefficient. *Agricultural Water Management* **49**, 153–161.

Li, Y., Anim, D. O., Wang, Y., Tang, C., Du, W., Yu, Z. & Acharya, K. 2014 An open-channel flume study of flow characteristics through a combined layer of submerged and emerged flexible vegetation. *Ecohydrology* **7**, 633–647.

Limerinos, J. T. 1970 *Determination of the Manning Coefficient From Measured bed Roughness in Natural Channels*. U.S. Geological Survey Water-Supply Paper 1898-B.

Liu, J., Chen, X., Zhang, J. & Flury, M. 2009 Coupling the Xinanjiang model to a kinematic flow model based on digital drainage networks for flood forecasting. *Hydrological Processes* **23** (9), 1337–1348.

Mahmoudi, M., Garcia, R., Cline, E., Price, R. M., Scinto, L. J., Wdowinski, S. & Miralles-Wilhelm, F. 2015 Fine spatial resolution simulation of two-dimensional modeling of flow pulses discharge into wetlands: case study of Loxahatchee Impoundment Landscape Assessment, the Everglades. *Journal of Hydrologic Engineering* **22** (1), D5015001.

Mao, Y., Ye, A., Liu, X., Ma, F., Deng, X. & Zhou, Z. 2016 High-resolution simulation of the spatial pattern of water use in continental China. *Hydrological Sciences Journal* **61** (14). DOI:10.1080/02626667.2016.1153102.

Moharana, S. & Khatua, K. K. 2014 Prediction of roughness coefficient of a meandering open channel flow using Neuro-Fuzzy Inference System. *Measurement* **51**, 112–123.

Noarayanan, L., Murali, K. & Sundar, V. 2012 Manning's 'n' co-efficient for flexible emergent vegetation in tandem configuration. *Journal of Hydro-Environment Research* **6**, 51–62.

Ou, G., Chen, X., Kilic, A., Shannon, B. H., Li, Y. & Samal, A. 2013 Development of a cross-section based streamflow routing package for MODFLOW. *Environmental Modelling & Software* **50**, 132–143.

Paiva, R. C. D., Collischonn, W. & Tucci, C. E. M. 2011 Large scale hydrologic and hydrodynamic modeling using limited data and a GIS based approach. *Journal of Hydrology* **406**, 170–180.

Petryk, S. & Bosmajian, G. 1975 Analysis of flow through vegetation. *Proceedings, American Society of Civil Engineers Journal of the Hydraulics Division* **101**, 871–884.

Reggiani, P., Todini, E. & Meißner, D. 2014 A conservative flow routing formulation: Déjà vu and the variable-parameter Muskingum method revisited. *Journal of Hydrology* **519**, 1506–1515.

Shangguan, W., Dai, Y., Liu, B., Ye, A. & Yuan, H. 2012 A soil particle-size distribution dataset for regional land and climate modelling in China. *Geoderma* **171**, 85–91.

Singh, V. P. 1996 *Kinematic Wave Modelling in Water Resources: Surface Water Hydrology.* John Wiley, New York.

Tang, M., Ren, Q. & Xia, D. 2008 The maximum power point study of solar cell based on genetic agorithm. *Power Electronics* **42**, 39–40.

Tóth, S. 2009 *River Capacity Improvement and Partial Floodplain Reactivation Along the Middle-Tisza-Scenario Analysis.* Report, Vituki Hungary, TU Braunschweig, Germany.

Wang, K., Ye, M. & Xu, Y. 2009 Proton exchange membrane fuel cell model optimization based on 1stOpt. *Chinese Journal of Power Sources* **33**, 698–700.

Wang, L., Wu, J. Q., Elliot, W. J., Fiedler, F. R. & Lapin, S. 2014 Linear diffusion-wave channel routing using a discrete Hayami convolution method. *Journal of Hydrology* **509**, 282–294.

Xia, J., Wang, G., Tan, G., Ye, A. & Huang, G. 2005 Development of distributed time-variant gain model for nonlinear hydrological systems. *Science in China Series D, [Earth Sciences]* **48**, 713–723.

Yadav, B., Perumal, M. & Bardossy, A. 2015 Variable parameter McCarthy–Muskingum routing method considering lateral flow. *Journal of Hydrology* **523**, 489–499.

Yan, B., Gu, S., Liang, J. & Sun, H. 2015 The generalized Nash model for river flow routing. *Journal of Hydrology* **530**, 79–86.

Yang, D., Li, C., Hu, H., Lei, Z., Yang, S., Kusuda, T., Koike, T. & Musiake, K. 2004 Analysis of water resources variability in the Yellow River of China during the last half century using historical data. *Water Resources Research* **40**, W06502.

Ye, A., Xia, J. & Wang, G. 2006a A distributed kinematic routing model based on dynamical networks. *Yellow River* **2**, 26–28 (In Chinese).

Ye, A., Xia, J. & Wang, G. 2006b A distributed time-variant gain model applied to Yellow River (II): model test and application. *Engineering Journal of Wuhan University* **39** (4), 29–32 (In Chinese).

Ye, A., Duan, Q., Zhan, C., Liu, Z. & Mao, Y. 2013 Improving kinematic wave routing Land Model scheme in Community Land Model. *Hydrology Research* **44**, 886–903.

Yuan, H., Dai, Y., Xiao, Z., Ji, D. & Shangguan, W. 2011 Reprocessing the MODIS Leaf Area Index products for land surface and climate modelling. *Remote Sensing Environment* **115**, 1171–1187.

First received 31 October 2017; accepted in revised form 10 February 2018. Available online 28 February 2018